Effects of increased irradiance on biomass, photobiology, nutritional quality, and pigment composition of Arctic sea ice algae

Lars Chresten Lund-Hansen[1,2,*], Ian Hawes[3], Kasper Hancke[4], Nicole Salmansen[2], Johanne Raakjær Nielsen[2], Laura Balslev[2], Brian K. Sorrell[2]

[1]Arctic Research Center, Department of Bioscience, Aarhus University, DK-8000 Aarhus C, Denmark

[2]Aquatic Biology, Department of Bioscience, Aarhus University, DK-8000 Aarhus C, Denmark

[3]Coastal Marine Field Station, Waikato University, Sulphur Point, New Zealand

[4]Norwegian Institute for Water Research (NIVA), Research Centre for Coast and Ocean, Oslo, Norway

* Corresponding author: lund-hansen@bios.au.dk

ABSTRACT: Ice algae are key contributors to primary production and carbon fixation in the Arctic and light availability is commonly assumed to limit their growth and productivity. This study investigated photo-physiological responses in sea ice algae to increased irradiance during the spring bloom at Kangerlussuaq Fjord, West Greenland. During a 14-day field experiment, light transmittance through sea ice was manipulated to provide three under-ice irradiance regimes i.e. low (0.04), medium (0.08), and high (0.16) transmittances. Chlorophyll *a* decreased with elevated light availability relative to the control. Photosynthetic efficiency (Φ_{PSII_max}) showed an initially healthy and productive ice algae community (Φ_{PSII_max} > 0.6) with Φ_{PSII_max} decreasing markedly under high light treatments. This was accompanied by a decrease in the light utilization coefficient (α) and photosynthetic capacity ($rETR_{max}$), and a decrease in the ratio of MUFA:PUFA fatty acids. This was partly explained by a corresponding increase of photoprotective pigments (diadinoxanthin and diatoxanthin), and a development of mycosporine-like amino acids (MAAs) as identified from a distinctive appearance of a spectral absorption peak at 360 nm. After 14 days, *in situ* fluorescence imaging revealed significant differences in Φ_{PSII_max} between treatments of dark-adapted cells (i.e., those sampled before sunrise and after sunset), during diel cycles, with clear chronic photoinhibition in high and medium treatments. These data demonstrate the high sensitivity of spring blooming Arctic sea ice algae to elevated irradiance caused by loss of snow cover. This known loss will impact negatively on ice algae and their potential primary production and nutritional quality for higher trophic levels.

KEY WORDS: Ice algae, high light, photophysiology, pigments, fatty acids, changing Arctic, Kangerlussuaq, Greenland

1. INTRODUCTION

Sea ice algae are important primary producers in polar ecosystems, especially in the early spring, where they constitute the main carbon source for higher trophic levels during the ice-covered period (Gosselin et al. 1997, Pabi et al. 2008; Fernández-Méndez et al. 2015. Their development is a function of light, temperature, nutrient availability and salinity experienced during the growth season, and available light is particularly vital in controlling spring growth and timing of the ice algae bloom (Mock & Gradinger 1999, Campbell et al. 2014). The photobiology of sea ice algae is characterized by extreme shade adaptation and the ability to acclimate to very low light intensities (Mock & Gradinger 1999, Leu et al. 2010, Galindo et al. 2017), with recent studies of active photosynthesis and growth at irradiances as low as 0.2 µmol photons m^{-2} s^{-1} (Hancke et al 2018). Conversely, they are highly susceptible to photoinhibition and photodamage at high irradiances (Lund-Hansen et al. 2014, Kauko et al. 2018) especially during sudden increases in irradiance associated with events such as snow melt (Hawes et al. 2012). Unlike phytoplankton, in which photoinhibition can be ameliorated by vertical movement in the water column by advection of water masses and fluctuating irradiance, ice algae are fixed in position under the sea ice and are unable to avoid whatever irradiance is transmitted to the underside of the sea ice. Several recent studies have documented losses of sea ice algal biomass and changes in species composition following an increased irradiance (Leu et al. 2010; Lund-Hansen et al. 2014), and there are also concerns that photodamage and stress may affect their nutritional quality and hence contribution to higher trophic levels (Leu et al. 2010). Light availability to the sea ice algae community is primarily a function of snow cover, as snow with its high albedo (> 0.8) and

scattering coefficients efficiently reduces light transmittance of photosynthetically active radiation (PAR) (Mundy et al. 2007, 2011; Hancke et al. 2018, Lund-Hansen et al. 2018. However, recent decades of meteorological data demonstrate a decrease in snow cover thickness in the Arctic Ocean related to climate change (Warren et al. 1999). Snow depth has decreased by 37% in the western Arctic and 56% in the Beaufort and Chukchi Seas based on nearly 40 years of observations (Webster et al. 2014). This decrease has been related to global warming, with a later freeze-up of ice during autumn and accordingly a shorter period for snow to accumulate on the ice, as most of the snowfall occurs during autumn (op. cit). The thinning of the snow cover and decrease in the minimum summer ice extent has led to suggestions of earlier and higher annual pelagic primary production (Assmy et al. 2017; Kauko et al. 2018) as observed on the summer ice-free Arctic shelfs (Arrigo et al. 2008), and as projected for an ice-free Central Arctic Ocean in summer (Lund-Hansen et al. 2020). The climate-driven shift to less multi-year and more annual first-year sea ice during the Arctic summer with less snow cover will also increase PAR availability over the growth season (Nicolaus et al., 2012). The possibility of ice algae experiencing photoinhibitory irradiances is therefore also enhanced, and their persistence in sea ice will depend on their ability to acclimate to both short- and long-term changes in irradiance. Key photophysiological mechanisms involved in ice algae light acclimation include changes in pigment composition, including chlorophyll content and synthesis of photoprotective carotenoids (Petrou et al. 2011). The accumulation of UV-absorbing mycosporine-like amino acids (MAAs) is also a known photoprotective mechanism in diatoms (Helbling et al. 1996, Piiparinen et al. 2015). A key indicator of physiological condition and photoacclimation *in situ* in recent studies has been the maximum quantum

yield of photosystem II (Φ_{PSII_max}) and photosynthesis-irradiance (*P-E*) responses as revealed by pulse-amplitude modulated fluorescence (PAM) methods (Hawes et al. 2012, Lund-Hansen et al. 2014). These variable fluorescence techniques can also assist with characterizing how algae acclimate to changes in irradiance experienced over periods of days to hours, for instance by applying photosynthesis-irradiance response curves or from short term acclimation revealed by rapid light curves (RCLs) (Ralph & Gademann 2005). In sea ice algae, the maximum photosynthetic efficiency defined by Φ_{PSII_max} is a highly sensitive indicator that typically increases from < 0.2 to > 0.5 during the spring bloom in healthy growing cells, and decreases rapidly in response physiological stressors, as for instance to prolonged elevated irradiance. The overall objective of this study was to investigate photophysiological acclimation in a land-fast first-year sea ice algae community during spring. Specifically, we aimed to test how manipulating snow cover thickness elevated the light availability and its effects on four important features of the ice algal community. These were (1) the temporal development and degree of photoinhibition experienced by the ice algal community, (2) the rate at which the photoprotective mechanisms of the community respond to photoinhibition and whether there is a specific sequence of their manifestation, (3) how increased light affected photophysiological parameters, and (4) the consequences of photophysiological stress on algal fatty acid synthesis. The latter is an effect that will have consequences for the quality of feed to the food web with ice algae being the primary producers of carbon.

110

111 ## 2. MATERIALS AND METHODS

112 ### 2.1 Study site and experimental design

113 The experimental site is on first-year level sea ice at Kangerlussuaq (66° 57.33'N, 50°
114 57.09'W), a 180 km long fjord-type estuary (Lund-Hansen et al. 2014) near the Arctic
115 Circle, west Greenland (Fig. 1). The area has a continental climate due to the nearby
116 Greenland ice cap with low winter minimum average winter temperatures of -15 to -25 °C
117 and precipitation of ~5 mm month^{-1} during December–July (www.altmetstat.com). The
118 estuary is ice-covered between October and early June with a snow thickness of ~0.5–
119 0.7 m (Lund-Hansen et al. 2014). It is governed by a strong, highly turbid meltwater
120 outflow (Lund-Hansen et al. 2010) from the Greenland Ice Cap (Hasholt et al. 2012)
121 between July and September. There is no inflow of freshwater to the estuary during winter
122 and spring. The tide is diurnal with a maximum spring tide of about 2-3 m (Nielsen et al.
123 2010). Water depth at the sampling site is ~120 m and the experiment was carried out in
124 March 2016.

125 The experimental design was a 14-day time series with ice algae subjected to three
126 irradiance regimes, i.e. two perturbation sites and a control with 400%, 200% and 100%
127 irradiance transmission relative to ambient conditions. The ~50 mm-deep snow layer was
128 cleared from two rectangular (12 × 4 m) areas of the fjord sea ice on Day 0 of the study.
129 One of these areas was covered with a neutral density semi-transparent tarpaulin that
130 provided 200% under-ice PAR compared to an adjacent control area of equal size that
131 was undisturbed, retaining the 50 mm snow cover (Fig. 2). The remaining cleared area

132 provided 400% irradiance compared to the control. Sampling areas were aligned east to
133 west to maximize exposure to irradiance and avoid disturbance of the light climate as
134 sampling progressed westwards. Two recently calibrated Odyssey PAR loggers
135 (www.odyssey.com) were placed immediately below the ice in the 200% and 400% areas.
136 A Li-Cor LI-192 PAR sensor was placed below the ice in the control area together with
137 two surface (LI-191) PAR sensors for measuring downwelling PAR and reflected PAR to
138 derive the surface albedo. Sensors were connected to a datalogger, which also measured
139 air temperature at 1 m above the surface. All loggers recorded at 5 min intervals. Below-
140 ice spectral irradiance was measured with a recently calibrated TriOS Ramses ACC VIS
141 cosine-corrected hyperspectral radiometer (www.trios.com). The sensor had a spectral
142 resolution of 3 nm and was mounted on a remotely operated vehicle (ROV) (Lund-Hansen
143 et al. 2018a) deployed through a hole in the ice and connected to a surface PC running
144 the TriOS standard software.

145

146 **2.2 Sampling and ice core processing**

147 Ice cores were collected with a Kovacs 90 mm ice auger powered by a battery drill. The
148 ice cores were carefully retrieved and covered with a black cloth to protect them from
149 photodamage during sampling. The cores were placed in a small cradle and the bottom
150 30 mm removed under shade using a stainless steel saw. Samples were then transferred
151 to clean 1 L polyethylene buckets and transported in coolers to the laboratory at
152 Kangerlussuaq International Science Support (KISS) for further processing within 30 min.
153 Three samples were collected at each location from each area on sampling Days 0, 3, 9,

and 12 between 12 and 25 March 2016, with an additional day for *in situ* diel sampling of fluorescence imaging on Day 14 (27 March). Under-ice seawater samples (UIW) were collected immediately below the ice in 15 L clean polyethylene canisters using a bilge pump. Upon return to the laboratory, the 30 mm core bottom sections were thawed in filtered seawater at 4 °C at a ratio of 1:1 ice to water. As the relative merits of different pre-treatments for variable chlorophyll fluorescence experiments has been debated in recent studies, we carried out a pilot study to compare fluorescence yield in directly thawed ice (no seawater), and ice:seawater volumetric ratios of 1:1, 1:2, and 1:3. The volume of seawater had no effect on fluorescence results, except fluorescence yields were lower in ice thawed without seawater. The volume ratio of 1:1 was therefore chosen to maximize sensitivity in analyses. UIW samples were filtered (Millipore Millex-GP hydrophilic PES 0.22 µm) and frozen in the dark at -18 °C for transport back to Denmark for analyses. Analyses of ammonia, nitrate + nitrite, silicate, and dissolved reactive phosphorus were conducted on the samples using a Skalar San Plus auto-analyser with a Skalar matrix photometric detector at Department of Bioscience, Roskilde, Denmark, using modified protocols of Grasshoff et al. (1983).

2.3 Variable Chlorophyll Fluorescence

Variable chlorophyll fluorescence measurements on ice algae were studied from thawed ice cores using a Phyto-PAM variable fluorometer (Heinz Walz GmbH, Effeltrich, Germany), as described by Schreiber et al. (1986). The instrument was placed in a darkened laboratory and a temperature control unit (Walz US-T) secured the temperature

inside the cuvette at 4 °C. The variable fluorescence signal was corrected for background autofluorescence by subtracting the fluorescence from a 0.2 µm filtered subsample. The technique is based on light saturation pulses with the variable fluorescence F_v given by $F_v = F_m - F_o$, where F_o is the minimum chlorophyll fluorescence and F_m is the maximum fluorescence yield of dark-acclimated algae cells after exposure to a strong (>1500 µmol photons m^{-2} s^{-1}) blue light pulse. The saturation pulse method is described in further detail by Schreiber et al. (1986). Rapid light curves (RLCs) were measured to derive the light utilization parameter (α), the onset of light saturation (E_k), and the maximum relative electron transfer rate ($rETR_{max}$). RLCs are based on a stepwise increase in actinic light intensities applied to the sample with 30 seconds at each intensity step interrupted by a saturation pulse (Schreiber 2004; Ralph & Gademann 2005). The Platt et al. (1980) equation was used to model α, E_k, and $rETR_{max}$ using the non-linear regression function of SigmaPlot version 12.0 (Systat Software Inc., San Jose, CA, USA).

Variable chlorophyll fluorescence was also measured *in situ* on freshly collected cores over a diel cycle at the end of the experiment (27 March, after Day 14) by fluorescence imaging with a Walz Imaging-PAM fluorometer (Hawes et al. 2012). The imaging-PAM fluorometer provides a two-dimensional 32 × 24 mm image of the algae distribution and their physiology from which photosynthetic parameters can be obtained. Further details of this method are given in Hawes et al. (2012). Here we applied the technique to derive diel cycles of Φ_{PSII}, the effective fluorescence yield of photosystem II at the immediately prevailing irradiance. Three replicate ice cores were collected from each of the three treatment areas (control, 200% and 400%) using a Kovacs ice auger. Samples were collected at 06:00, 08:00, 10:30, 13:00, 15:00, and 17:00 and great care was taken to

protect the samples from ambient light using a black cloth. The ice core was placed in the cradle and the lowermost 30 mm removed using a stainless steel saw. Samples were imaged immediately after sampling in a dark measuring box housing the imaging-PAM fluorometer, placed inside a tent on the ice. The 17:00 samples were also returned to the laboratory in a darkened cooling box and re-imaged at 19:30 and 21:30 to follow the recovery of the Φ_{PSII} in continuous (post-sunset) darkness.

2.4 Pigment analysis and species composition

For pigment analysis the ice samples were diluted (1:1) with a known volume of filtered (0.2 µm) seawater from below the ice to avoid osmotic stress (Garrison & Buck 1986; Rintala et al. 2014) and thawed in the dark at 4 °C for 24 h. After thawing, an exact volume (50-100 mL) was filtered on to GF/C Whatman filters with a nominal pore size of 1.2 µm for chl *a* and filters stored at -20 °C until returned to Denmark where they were stored at -80 °C until processing. For extraction of chl *a*, 5 mL 96% ethanol was added to the filter. The mix was sonicated for 10 min and stored at 5 °C for 20 h. After extraction the samples were re-sonicated and centrifuged for 10 min at 4000 rpm. The supernatant absorbance was determined as FSU with a Turner 10-AU fluorometer calibrated with chl *a* standards and concentrations obtained by the linear relationship between chl *a* and FSU. For further details on the method see Lund-Hansen et al. (2014).

For high-performance liquid chromatography (HPLC) analysis a volume of ~350 mL thawed ice was filtered. The extraction was as per Hou et al. (2011) with slight modifications. The HPLC filters were placed in cryovials and stored in a liquid nitrogen

dry shipper (-192 ºC) until returned to Denmark where samples were stored at -80 ºC until processing. Filters were cut into small pieces and 2 mL 100 % cold methanol was added. The mix was sonicated for 30 s and kept in darkness at -20 °C. The extract was then filtered through 0.22 µm Q-Max® RR Syringe filters directly to HPLC vials. The extract was injected using an automated sampler into a Thermo Scientific Ultimate 3000 high-performance liquid chromatograph fitted with a diode array detector, with the detector signal monitoring at λ = 450 nm (Hou et al. 2011). A Kinetex 2.6 µ C8 100 Å column (100 mm x 3.0 mm ID) was used to separate the samples, with a mobile phase A as 100% methanol:1M ammonium acetate (70:30) and a mobile phase B as 100% methanol. The gradient of the mobile phase was started with 80% of A (20% of B), and then linearly decreased to 5% of A (95% of B) in 10 min. Finally, it was returned to initial conditions for 2 min and held for an extra 2 min. The flow rate was 0.5 ml min^{-1}, the column oven was set to 50 °C, and the injection volume was 20 µL for the most concentrated pigments; for other samples this was reduced to 5 or 0.5 µL. We focus here on fucoxanthin (fuco), diadinoxanthin and diatoxanthin (ddx+ddt), as the dominant carotenoids in the ice-algae. For comparison between samples, the HPLC pigment concentrations were normalized to chl *a*.

Subsamples of 75 mL from each treatment of the thawed ice were preserved with acidic Lugol's iodine (final concentration 1%). The Utermöhl method (1958) was applied for enumeration of cell densities. Samples were mixed 25 times and poured into 10 mL settling chambers for 20-24 h. Counting was done using an inverted microscope (Nikon Eclipse Ts2R-FL) equipped with phase contrast. Counting was done in diagonals or half-chambers. If possible at least 400 cells were counted independent of area.

2.5 Spectral absorption

Samples for spectral absorption were taken from the diluted (1:1) and thawed ice cores. Volumes of ~250 mL were filtered onto Whatman GF/C filters including four additional filtered samples of sea water to be used as blanks. All samples were packed, marked individually and stored at -20 °C and transported back to Denmark and then stored at -80 °C until processing. Optical density was measured on the filters between 350 and 750 nm on a Shimadzu UV 2600 spectrophotometer with an attached integrating sphere. The optical density of algae (OD_p) was measured by soaking the filters in 50-100 µL MQ-water in 5 min in darkness before the samples were placed in the spectrophotometer to obtain the spectral absorption coefficient for phytoplankton $a_\varphi(\lambda)$. Afterwards the filters were de-pigmented by adding 5-15 mL methanol for 3 h and the filters were dried and soaked in 150-170 µL MQ-water. The optical density of de-pigmented particles (OD_d) was then measured on the spectrophotometer. The spectral absorption coefficient - $a_\varphi(\lambda)$ - was then calculated as:

$$a_\varphi(\lambda) = \frac{2.303 * A_f * [OD_p(\lambda) - OD_d(\lambda)]}{\beta * V_f} \quad (1)$$

with A_f as the effective area of the filter (m^2), V_f the volume of the filtered sample (m^3). Both OD_p and OD_d are corrected for blanks, and β is set at 2, the correction for path length amplification within the glass fibre filter (Cleveland & Weidemann 1993; Mitchell 2002).

The spectral absorption coefficient $a_\varphi(\lambda)$ was divided by the chl *a* concentration of the sample to get the chl *a*-specific absorption coefficient $a^*_\varphi(\lambda)$.

2.6 Fatty acid analysis

Subsamples of 200-300 ml thawed ice were filtered onto 25 mm pre-combusted glass fibre filters (GF75 Advantec). The filters were transferred to cryovials and stored in a liquid nitrogen dry shipper (-196 °C) for transportation to Denmark and then stored at -80 °C until analysis. The fatty acid composition was determined after fatty acid methylation and analysis on a gas chromatograph equipped with a flame ionization detector (GC-FID). The filters were transferred to tubes and 2 mL sodium hydroxide added. This mixture was exposed to ultra-sonication for 20 min before extraction. 2 mL boron trifluoride in methanol (BF_3-MeOH) was added and methylated by boiling. 1 mL heptane with 0.01% (w/v) butylated hydroxytoluene (BHT) and 5 µL of internal standard (2% w/v C23:0 in heptane) were then added. The heptane phase of the sample was transferred to GC vials and analysed by gas chromatography (HP-7890 A, Agilent Technologies, CA, USA). Fatty acid methyl esters were separated and detected by the GC column Agilent DB wax 127-7012 (10 mm x 100 mm x 0.1 mm) from Agilent technologies (CA, USA). The oven temperature program was from the initial temperature of 160 °C increased by 10.6°C min^{-1} to 200 °C, held for 0.3 min, then increased by 10.6 °C min^{-1} to 220°C and held 1 min, then by 10.6°C min^{-1} to 240°C and held 3.8 min. A split ratio of 1:50 was used and the determination was made in duplicates. Fatty acids were identified by comparison of retention times with a mixture of standards, containing all the fatty acids identified in this study. Results were calculated as area % of total fatty acids.

286

287

288

2.7 Statistical analysis

289

290 Chl *a*, maximum fluorescence yield (Φ_{PSII_max}), RLC data and the ratio of MUFA to PUFA
291 were analyzed by 2-way (treatment and sampling date) ANOVA, with treatment as a fixed
292 factor and sampling dates as a random factor. *Post-hoc* Tukey HSD tests were then used
293 to evaluate when there were significant differences between treatments during the study.
294 Prior to ANOVA, data were checked for normality and homogeneity of variances with
295 Levene's test, and were log-transformed when necessary to correct for deviations from
296 these assumptions. All statistical analyses were performed with JMP Version 12.1.0 (SAS
297 Institute Inc., Cary, NC, USA).

298

3. RESULTS

299

3.1 Climatic conditions, optics and nutrient availability

300

301 The 14-day period of the experiment encompassed initial cold, clear weather over the
302 first five days, followed by a snowfall event and increased air temperatures (Fig. 2A). Daily
303 maximum downwelling PAR was 600 µmol photons m^{-2} s^{-1} during the initial five-day period
304 and increased to 900 µmol m^{-2} s^{-1} during the rest of the study (Fig. 2B). A similar pattern
305 was observed below ice at the perturbed sites but at reduced levels (Figs. 2C, 2D).
306 Maximum PAR irradiance varied between 10-30 µmol photons m^{-2} s^{-1} in the control area,
307 30-60 µmol photons m^{-2} s^{-1} in the 200% area, and 60-140 µmol photons m^{-2} s^{-1} in the

400% area. Light transmittances were 0.16 at the 400%, 0.08 at the 200%, and 0.04 at the control sites, respectively, which demonstrated how transmittance increased by 200% and 400% respectively at the perturbed sites. Sea ice thickness varied between 79 and 80 cm with no changes in ice thickness over time. The snowfall event of 18-19 March increased snow thickness from about 10 mm to 50 mm and reduced under-ice PAR at the control site to about 1% of downwelling PAR (Fig. 2D). Transmittances in the 200% and 400% treatments remained constant as we removed any drifting snow on a daily basis but left the control area undisturbed. Integration of daily PAR during the study period gave total PAR values of 7.4, 15.7, and 29.3 mol m^{-2} per day in the control, 200%, and 400% sites, respectively. Spectral irradiances below the ice measured on 13 March show a comparable gradient to PAR between the three areas and that relative spectral distribution was similar in the three areas. The UV-A intensities (W m^{-2}), obtained by integration of the spectral irradiance between 320-400 nm, reached 0.4, 2,0 and 3.7 W m^{-2} in the control, 200%, and 400% areas. Measured PAR levels from where the UV-A intensities were derived all complied with maximum PAR levels in each of the three areas: 21.1 (control), 66.5 (200%), and 121.0 (400%) µmol photons m^{-2} s^{-1}. The nutrient concentrations in the UIW were 3.60 (NO_3), 0.12 (PO_4), and 7.01 (SiO_2) µmol L^{-1}.

3.2 Responses of ice algal communities, pigments and Φ_{PSII_max}

Algal species composition was dominated by diatoms, but dinoflagellates and several small unidentified flagellates were also present. There was one unidentified and six identified diatom species (*Nitzschia longissima*, *Nitzschia frigida*, *Thalassiosira sp.*,

Bacillaria pax, *Entomoneis paludosa*, *Gyrosigma/Pleurosigma* sp.), dominated by the pennate *N. longissima*, *N. frigida*, and the centric *Thalassiosira sp.* (~1000-1500 cells mL^{-1}). Other taxa were few in numbers (< 100 cells mL^{-1}). There was a decrease in cell numbers of the unidentified diatom, from an average of 1500 to ~100 cells mL^{-1} along with a decrease in *Thalassiosira sp.*, in all three areas over the course of the experiment. The unidentified diatom was a comparatively small species about 10 µm length and 1-2 µm width. There was, in comparison, an increase in *N. longissima* from 963 to 1400 cells mL^{-1} in the 400% area between the start and end of the experiment, and similarly for *N. frigida*, which increased by 883 cells mL^{-1}. In summary, the overall number of cells did not change significantly during the course of the experiment.

ANOVA revealed significant effects of treatments on ice algae expressed as chl *a*, that developed over the course of the experiment (Table 1). There was no significant difference in chl *a* between the three areas at the start of the experiment, but by Day 9 chl *a* in both 200% and 400% treatments had fallen below the control treatment (Fig 3A). This difference persisted for the remainder of the experiment, with the 200% and 400% treatments not differing significantly from each other.

HPLC data showed that the ratio of the light-harvesting pigment fucoxanthin normalized to chl *a* concentration (fuco:chl *a*) did not differ significantly between treatments ($F = 1.25$, $P = 0.32$). However, this ratio was higher in ice algae (mean ± 1 SD of all samples = 1.97 ± 0.27) than in phytoplankton from the UIW (0.04 ± 0.02). Ratios of the light-protecting pigments diadinoxanthin and diatoxanthin to chl *a* (ddx + ddt:chl *a*) were significantly lower overall in the control (0.17 ± 0.02) than in the 200% (0.21 ± 0.06) and 400% (0.28 ± 0.09) treatments ($F = 3.31$, $P < 0.05$); these ice algal ddx + ddt:chl *a*

353 data can again be contrasted against low values (always < 0.01) in the under-ice
354 phytoplankton.

355 These community and pigment responses were accompanied by significant effects of
356 increased irradiance on Φ_{PSII_max}, the maximum dark-adapted yield, as measured in
357 Phyto-PAM samples (Table 1). Φ_{PSII_max} began to decrease in the 400% treatment already
358 by Day 6, and from Day 9 onwards was significantly different in all three areas, remaining
359 highest (> 0.60) in the control treatment, and ultimately stabilizing at particularly low yields
360 (< 0.50) in the 400% treatment (Fig. 3B).

361

362 **3.3 Rapid light curves**

363 Photosynthetic acclimation to differences in irradiance over time were also evident in
364 RLC data (Table 1, Fig. 4). ANOVA analysis of the RLCs revealed significant differences
365 in $rETR_{max}$ developing over the course of the experiment (Table 1, Fig. 4A). Initially
366 $rETR_{max}$ did not differ between treatments, but on Days 9 and 12 it had become
367 significantly lower in the 200% and especially in the 400% treatments (Fig. 4A). Significant
368 differences in the photosynthetic efficiency α were also evident by Day 12 (Table 1, Fig.
369 4B), with α becoming lower in the 400% treatment than the other treatments. The light
370 saturation irradiance E_k was, on the other hand, unaffected by the irradiance treatments
371 (Table 1, Fig. 4C).

372

373 **3.4 Spectral absorption**

There were two significant peaks in the normalized (670 nm) chl *a*-specific absorption coefficient $a^*_{chl\text{-}a}$ around 440 nm and 670 nm at all four samplings. There was, besides these two consistent peaks, a very significant development of strong absorption peaks centered at 360 nm in both the 400% and 200% treatments (Fig. 5). There were, on the other hand, no changes in the absorption at 360 nm in the control treatment (Fig. 5).

3.5 Fatty acids

PUFAs were the dominant (28-36%) fatty acids with 20:5(n-3) (10-15%) and 22:6(n-3) (4-5%) as the dominant PUFAs. MUFAs were less dominant (19-31%), dominated by 16:0 (15-18%), 16:1(n-7) (15-18%), 14:0 (4-8%), and 18:0 (2-5%). There was a significant decrease in PUFAs in all three areas and especially after Day 6 from about 35% to 27%, and a parallel increase in MUFAs from about 19% to 25% during the study period, shown for the 400% area (Fig. 6). SAFA content was close to constant and similar in all three areas at about 26% of total fatty acid composition. The MUFA:PUFA ratio increased over time from about 0.5 to about 0.9, and ANOVA revealed a significant lower MUFA:PUFA ratio in the 200% and 400% areas compared to the control area by Days 12 and 14 (Table 1, Fig. 6). The MUFA/PUFA ratio increase was linked to an increase in the MUFA content of 16:1(n-7), which increased by 12.9% point between start and end of experiment in the 400% area, and a parallel reduction of the PUFAs 20:5(n-3) and 22:6(n-3) by 4.6 and 2.7.

3.6 Response times

Significant changes in fluorescence yield (Φ_{PSII_max}) occurred after Day 6, but not until after 9 and 12 days from the beginning of experiment for electron transfer rates ($rETR_{max}$) and light utilization (α), respectively. Changes in pigment composition occurred after Day 6 along with the development in MAAs, whereas a significant loss of chl *a* first occurred at Day 9 concurrent with a loss of cells of the unidentified pennate diatom. Changes in fatty acid compositions occurred on Day 12. There were no differences in the response time of photoprotective parameters, as compared to the photophysiological parameters. It is notable that the response time of maximum fluorescence yield (Φ_{PSII_max}), which is the major photophysiological parameter in fluoresence based analyses, was similar to those of the pigments and MAAs.

3.7 Diel cycles of photosynthetic efficiency

In situ fluorescence imaging at the end of the experiment (Day 14) identified diel cycles in Φ_{PSII} with Φ_{PSII} decreasing in all three areas in response to the diurnal increase in under-ice PAR, and conversely recovering between noon and sunset as irradiance decreased (Fig. 7A). Φ_{PSII} continued to increase after sunset before returning to dark-acclimated Φ_{PSII_max} levels between 20:00 and 21:00 h in all three treatments. Fluorescence yields were significantly different between the three treatments throughout the diel cycles (Table 1). Even the dark-acclimated Φ_{PSII_max} values before sunrise and after sunset were highest in the control treatment and lowest in the 400% treatment, and

418 daytime irradiance caused even greater difference in Φ_{PSII} between treatments. There
419 was a uniform exponential ($r^2 = 0.91$) decrease in Φ_{PSII} vs irradiance across all data points
420 from all three treatments (Fig. 7B). These data from 27 March at the end of the experiment
421 reflect the cumulative light history of algae exposed to 14 days of the different PAR levels
422 in the three treatments.

423

424 **4. DISCUSSION**

425 **4.1 Snow-clearing experiments and light treatments**

426 In this study we were able to establish three very distinct irradiance regimes for ice algae
427 communities under sea ice, with differences in light availability driven by the difference in
428 sea-ice snow cover due to its strong light attenuation properties (Mundy et al. 2005). The
429 unperturbed control site, elevated 200% and elevated 400% treatments provided a
430 gradient and an intensive *in situ* time series over 14 days through which we were able to
431 determine the time required for significant photoinhibitory effects to develop in an ice
432 algae community, and the extent to which photoprotective responses could ameliorate
433 these effects. To our knowledge, this is the first study to measure photophysiology using
434 variable fluorescence, community structure, pigment composition, MAA development,
435 and food quality simultaneously in the same study.

436 Ice algae communities are adapted (i.e. long-term genetically customized) to very low
437 light levels (Arrigo et al. 2008; Hancke et al. 2018) due to their position below sea ice,
438 which is often covered with snow. Snow is a strong attenuator of irradiance (Perovich et
439 al. 2017) relative to sea ice itself, with PAR attenuation coefficients of 11.9 and 0.84 m^{-1}

respectively (Lund-Hansen et al. 2018). This is driven by the high albedo of snow (0.8-0.9) where snow transmittance, besides thickness, also depends on water content, compaction, and age (Perovich et al. 2017). This emphasizes the importance of the snow cover as the critical regulator of under-ice irradiance and hence light availability to ice algae. Ice algae biomasses are often negatively correlated with snow cover thickness (Leu et al. 2015) as is their primary production, a vital contribution to higher trophic levels during the ice-covered spring before commencement of the pelagic production (Mundy et al. 2014). In this context, snow removal on sea ice is an appropriate experimental design for studying the effects of elevated irradiances over time and photophysiological and photoprotective responses of ice algae communities (Juhl & Krembs 2010; Lund-Hansen et al. 2014). Below-ice PAR levels remained quite stable during the experimental period, and any possible effects of the observed increase in PAR levels will only have amplified the effects related to increased PAR. The snowfall related decrease in under-ice maximum noon PAR in the low light area from about 30 to 10 µmol photons m^{-2} s^{-1}, would presumably have enhanced experimental effects, by broadening the interval between low (10 µmol photons m^{-2} s^{-1}) and high (140 µmol photons m^{-2} s^{-1}) under-ice maximum mid-day PAR

Indeed, snow removal has resulted in reduction in photosynthetic activity and algal biomass in some previous studies. A combined laboratory and field study of snow thickness and ice algae photosynthesis observed significant effects at PAR interval levels up to 100 µmol m^{-2} s^{-1} (Juhl & Krembs 2010). Removal of a 10 cm thick snow cover - also in Kangerlussuaq - increased under-ice maximum PAR from about 30 to 250 µmol m^{-2} s^{-1}, causing significant decreases in photosynthetic parameters, chl *a* concentrations, and

463 an entirely changed species composition (Lund-Hansen et al. 2014). Other ice algae
464 studies have also shown significant changes in photosynthetic performance and chl *a*
465 concentrations relative to different under-ice PAR levels between 0.02 - 100 µmol m^{-2} s^{-1}
466 (Grossi et al. 1987). This demonstrates that the PAR levels in the present study (10-140
467 µmol m^{-2} s^{-1}) are within the range in which ice algae have been observed to respond to
468 changes in PAR. The present under-ice levels are similar to other Greenland (Mikkelsen
469 et al. 2008; Lund-Hansen et al. 2018) and Canadian Arctic ice algae study sites (Mundy
470 et al. 2014; Campbell et al. 2014) with comparable snow cover thickness. This further
471 demonstrates the relevance of the present results for the larger regional scale of the
472 Arctic.

473

474 **4.2 Effects of light on ice algal chl *a* and species composition**

475 The sea ice chl *a* concentrations (0.5-1.5 mg chl *a* m^{-2}) in this study were similar to
476 previous concentrations described in Kangerlussuaq in March (Hawes et al. 2012; Lund-
477 Hansen et al. 2014). They are nevertheless up to three times higher than other Greenland
478 fjords such as Kobbefjord (0.5 mg chl *a* m^{-2}), south of Kangerlussuaq, and on the high
479 Arctic east coast at Young Sound (0.5 mg chl *a* m^{-2}) at the same time of year (Rysgaard
480 et al. 2001). These chl *a* concentrations in Greenland are, however, relatively low
481 compared to other Arctic sites at maximum bloom (20-40 mg chl *a* m^{-2}, e.g., Leu et al.
482 2015).

483 The wide range in species composition and biomass of sea ice algae recorded in polar
484 regions is testimony to the sensitivity of these communities to relatively small variations

485 in the immediate light climate they experience, and the history of irradiance they have
486 been subject to during the growth season. Any particular sampling programme is a
487 snapshot of a community integrating a light history of days or weeks in advance, and
488 almost all previous studies have demonstrated that even small changes in available PAR
489 lead to dramatic community changes during the spring bloom season. In this study, chl *a*
490 remained unchanged in our control area, in contrast to the significant decrease from about
491 1.2 to 0.8 mg chl *a* m^{-2} at the perturbed sites with elevated under ice irradiance. We
492 previously observed that exposure of under–ice algae to increased PAR from about 30 to
493 250 µmol m^{-2} s^{-1} over a ten-day period caused a significant decrease in chl *a* from about
494 0.8 to less than 0.05 mg chl *a* m^{-2}, specifically related to the pennate diatom *Fragilariopsis*
495 *oceanica* leaving the ice (Lund-Hansen et al. 2014). In the present study, the initial
496 community was very different from that of 2011 and the chl *a* decrease was accompanied
497 by reduced representation of an unidentified diatom along with a *Thalassiosira sp.* that
498 decreased in numbers during the study period. These are both pennate diatoms, motile
499 in the sea-ice matrix (Horner 2018), and hence the decreased chl *a* could reflect that
500 these algae can actively respond to higher PAR levels by leaving the ice. The ice algae
501 species composition was here instead dominated by the two *Nitzschia* species *N.*
502 *longissima* and *N. frigida*, and the unknown diatom, which is quite different from the
503 composition in 2011 that was initially dominated by *Achnanthes taeniata* and
504 *Fragilariopsis oceanica* (Lund-Hansen et al. 2014). Juhl & Krembs (2010) showed in
505 laboratory experiments that *N. frigida* can persist and thrive at relatively high PAR, which
506 might explain the observed increase in *N. frigida* numbers from 1428 to 2311 cells mL^{-1}
507 between the start and end of this experiment in the 400% area. The different species

composition compared to 2011 and the presence of the high-light tolerant *N. frigida* suggests that the experimental site had been exposed to periods of high light before the experimental period. This is supported by observations of a week-long period in February 2016 where the ice was nearly snow-free due to snowmelt (Rika Møller, KISS Manager, pers. com). It is likely that the absence of snow in February increased under-ice PAR, which then promoted a different species composition and the occurrence of *N. frigida* in higher numbers compared to 2011, where a hard-frozen 10 cm thick layer of snow covered the sea ice (Lund-Hansen et al. 2014).

4.3 Algal photobiology and photoprotection

The sensitivity of ice algal photophysiology to changes in irradiance is a recurring feature in understanding their development, persistence and species composition (Campbell et al. 2014; Kauko et al. 2018). Increasing spring irradiance allows algal development in a wide range of ice habitats, and generally, habitats with higher light availability have higher algal biomass as the spring bloom persists (Leu et al. 2015). However, ice algae are necessarily strongly shade-adapted organisms given their need to develop under extreme low irradiance under snow-covered ice. Their shade adaptation and acclimation makes them prone to photoinhibition under elevated irradiances exceeding the acclimated levels, especially as they are fixed in position and hence unable to mechanically avoid excess irradiance, as for instance benthic microalgae that migrate downward in sediments (Haro et al. 2019). The community response to sudden increases in irradiance is typically a rapid decrease in chl *a* content and increased synthesis of photoprotective pigments

(Nymark et al. 2009; Lavaud and Goss 2014). Community responses can reflect several processes, including (i) decreased cellular pigment content (both chl *a* and other light harvesting pigments), (ii) mortality or emigration of sensitive taxa from the ice, and (iii) flushing and sloughing of cells from the ice if elevated irradiance leads to warming and/or thawing of the ice. The ice algal community at Kangerlussuaq during the spring bloom is, however, restricted to the skeletal layer on the underside of the ice (Lund-Hansen et al. 2016), and there is no evidence for any such physical losses as the ice remained cold and intact. Nor is there any sign of nutrient or temperature limitation for the ice algae community during the spring period, given the excess nutrients available below the ice at this time. Nutrient concentrations in the UIW during the study were similar to concentrations measured previously at the same site and time of year (Lund-Hansen et at. 2014). In the ice-free summer period, NO_3 can fall to 0.61 µmol L^{-1} in August due to phytoplankton N demand (Lund-Hansen et al. 2018), but the low biomass and high NO_3 concentrations in March are consistent with ice algae and phytoplankton spring blooms yet to commence.

In the current study, the constant total cell numbers throughout the 14-day period accompanied by decreased chl *a* and decreased fuco:chl *a* ratio and change in species composition indicates acclimation to higher light by those taxa persisting after snow removal and also high irradiance acclimation by the new colonisers (*Nitzschia longissima* and *N. frigida*). The increased ddx+ddt:chl *a* ratio and appearance of absorption peaks consistent with mycosporine-like amino acids (MAA) development (see below) are both clear indicators of a community that is attempting to manage irradiances exceeding its light harvesting capacity. To our knowledge, the present data are the first to identify

553 simultaneous acclimation by these two mechanisms at the same time during an *in situ*
554 experiment.

555 As the ddx+ddt:chl *a* ratio and MAA development are suggestive of a response to
556 photoinhibition, this should be evident also from measuring photophysiology responses
557 of the algae community. Such can be achieved using variable chlorophyll fluorescence
558 methods, which have become an important technique for understanding ice algal
559 photoacclimation responses (Hawes et al. 2012; Lund-Hansen et al. 2016). Our
560 complementary application of PAM-fluorometry using both thawed ice in the Phyto-PAM
561 and *in situ* fluorescence imaging provides solid insight into the development and
562 photophysiological effects of photoinhibition during elevated light regimes. Notably, the
563 parameter that responded most rapidly to increased irradiance was Φ_{PSII_max}, decreasing
564 significantly already by Day 6, before any change in pigment composition or MAA
565 development were evident. This confirms the importance of Φ_{PSII_max} as a sensitive and
566 early indicator of ice algal activity and production. Increasing Φ_{PSII_max} values during
567 spring blooms are useful rapid indicators of increasing activity during the earliest onset of
568 the bloom (Hancke et al. 2018), and here in detecting progressive photoinhibition. The
569 Φ_{PSII_max} values > 0.6 at the control site were as high as any recorded for sea ice algae
570 (Hawes et al. 2012), indicting a healthy and highly productive community. At the perturbed
571 sites, the continuous decline of Φ_{PSII_max} demonstrated how the photoprotective
572 mechanisms were insufficient to restore Φ_{PSII_max} to its pre-perturbed level. The
573 subsequent decrease in $rETR_{max}$ and α and lack of increase in E_k further emphasise the
574 inability of the community to fully acclimate to the elevated irradiances at the perturbed
575 sites.

The diel cycles of Φ_{PSII} established by *in situ* fluorescence imaging confirm chronic photoinhibition as a response to elevated irradiance, demonstrated by (i) the failure of Φ_{PSII} in the two snow-cleared areas to return to similar Φ_{PSII_max} values to the control in the dark, and (ii) the very low values of Φ_{PSII} at the highest irradiances. Overall, the effects observed are of a community that becomes rapidly photoinhibited by the sudden increases in irradiance, that attempts to manage this by changes in pigment and MAA content, but which is unable to prevent persistent, severe photoinhibition in these conditions.

The data indicate an increased cellular investment in MAAs at elevated irradiance, as observed from a clear absorption peak at 360 nm in the 200% and 400% treatments, but not at the control site. Although we did not measure MAAs directly, there is strong evidence in the literature that such absorption peaks are related to absorption of MAAs in algae (Riegger & Robinson 1997, Ayoub et al. 2012, Piiparinen et al. 2015). Algae synthesize MAAs in their cells as protection against UV radiation; in dinoflagellates UV-B tends to initiate production of MAAs (Caretto & Carignan 2011), whereas high MAAs in diatoms are generally caused by UV-A radiation (Helbling et al. 1996). MAAs have absorption peaks between 309 and 362 nm, whereas the absorption at 360 nm is related to palythene (Carreto & Carignan 2011). The MAA pool in sea ice changes over time and is clearly dependent on exposure to high irradiance, whether the algae are in melt ponds or at the bottom of the sea ice with a snow cover (Elliott et al. 2015). Our samples were only scanned between 350 and 750 nm, so there are no data on the total MAA pool in Kangerlussuaq, but we observed a clear and strong absorption peak at 360 nm, which gradually developed over time and became more pronounced, and especially in the 400%

area. Palythene absorption peaks have also been found in phytoplankton in a high (~1900 m.a.s) alpine lake exposed to strong UV-radiation (Ficek et al. 2013). Maximum UV-A intensities reached 0.4, 2.0, and 3.7 W m^{-2} in the three irradiance treatments. After we removed the 4-5 cm thick snow cover from the two manipulated areas that were kept snow free during the study period, the ice algae in the 400% treatment abruptly became exposed to UV-A levels that were nearly ten times higher than in the control area. The timescale for MAA development is not well understood and here it took about 6 days before a statistically significant development of MAAs was identified from a 360 nm absorption peak. Chl *a* concentrations at Day 14 were slightly lower in the 400% and 200% areas compared to Day 9, where this reduction might have been related to the development of the MAAs as metabolic costs of an MAA production is similar to those of chl *a* (Shick et al. 2002). The filter pad technique has been questioned for quantification of MAA concentrations in phytoplankton, as MAAs can be released from the cells when thawed and washed out by rinsing of filters giving erroneous and comparatively low MAA concentrations (Laurion et al. 2003). Our filters were only wetted and all Milli-Q water was absorbed by the filter prior to spectrophotometer analyses and compounds thus retained inside the filters. We would not have observed any gradual increase in MAAs absorption in both 200% and 400% light areas if MAA compounds had actually been lost prior to analyses. In any case, the data qualitatively demonstrate the increased absorption by MAAs in relation to increased UV-A. Studies have shown that dinoflagellates are relatively more susceptible to synthesising MAAs when exposed to UV-A compared to diatoms (Karentz et al. 1991; Sinha et al. 2007). We observed different algae groups (e.g. haptophytes, euglenophytes, and small unidentified flagellates) in our samples including

dinoflagellates but they were not quantified as diatoms overwhelmingly dominated. Dinoflagellates were present in the sea ice, but in low abundances relative to diatoms, which indicates that the MAAs were most likely synthesized by the diatoms. High MAAs have also been found at other Arctic sites where diatoms completely outnumbered dinoflagellates (Elliot et al. 2015), though laboratory studies have pointed out that MAA synthesis can also vary between diatom species (Helbling et al. 1996).

4.4 Effects on fatty acid composition

Several studies have documented the high importance of fatty acids in ice algae, particularly PUFAs and MUFAs, for higher Arctic trophic levels including zooplankton (Arendt et al. 2005), polar cod (Doreen et al. 2017), and for the entire Arctic food web (Budge et al. 2008). PUFAs are essential dietary components that are only synthesized by algae (Sargent et al. 1995). Concentrations and changes of fatty acid composition are linked to algae species composition, nutrient concentrations and irradiance (Leu et al. 2006), as demonstrated by a general negative correlation between PAR levels and PUFA content (Leu et al. 2010). Our study is one of the first *in situ* studies of fatty acids with a high time resolution (every 3 days) at three different controlled under-ice PAR levels covering a 14 day-period, and identified significant effects of light treatments on fatty acid composition. PUFA content decreased similarly in all three PAR treatments over time from about 38 to 26%, mainly by reduced contents of the essential lipids 20:5(n-3) and 22:6(n-3). MUFA content increased in the three treatments from about 16 to 28%, linked to an increase in 16:1(n-7) but with no changes in SAFA content. The reduction in PUFA

and specifically 20:5(n-3) and 22:6(n-3), and the increase in MUFA 16:1(n-7) were in fact very similar to observations by Leu et al. (2010), who attributed the changes to increased PAR. Here PUFAs decreased and MUFAs increased in all three PAR treatments and at similar PAR levels as in the Leu et al. (2010) study. The fatty acids 20:5(n-3) and 22:6(n-3) are designated markers for diatoms and flagellates, respectively (Reuss & Poulsen 2002). The decrease in 20:5(n-3) might be attributed to the corresponding decrease in cell numbers of the unidentified diatom, which decreased from about 2000 to about 100 cells mL^{-1} from the beginning to the end of the experiment. However, the unidentified diatom was very small, about 10 µm long, whereby biomass loss and then loss of fatty acids was restricted based on the power function relationship between cell size and carbon and thus chl *a* (Meunden-Deuer et al. 2001). Two other diatom species, *N. longissima* and *N. frigida* increased by a total of about 700 cells mL^{-1} in the high light area at the same time. The disappearance of the unidentified diatom from the ice was gradual and at similar rates in all three treatments, but this diatom was replaced by other species of diatoms, which strongly indicates that observed changes in PUFA and MUFA could not be linked to the loss of diatoms. Fatty acid composition changes can be attributed to variable nutrient concentrations (Leu et al. 2010) but nutrients were unlimiting in March during this study, as noted above. The MUFA:PUFA ratio increased in all three areas over time and most strongly in the high light area, linked to an increase of 13% in MUFA 16:1(n-7) and a decrease of 7.6% in the PUFAs 20:5(n-3) and 22:6(n-3). The significantly higher MUFA:PUFA ratio in the high light area indicates that observed changes in fatty acid compositions were linked to PAR. UV-B has specifically been linked to changes in fatty acid composition as UV-B can restrict ATP production in algal cells (Vosjan et al. 1990),

667 where synthesis of PUFAs requires relatively larger amounts of ATP compared to those
668 of MUFAs and PUFAs (Thompson et al. 1992). UV-B can reduce the levels of the omega-
669 3 PUFAs EPA and DHA, though effects were dependent on algae species and diatoms
670 were least affected (Wang & Chai 1994). The UV-B induced reduction in EPA and DHA
671 has also been observed in other studies (Hessen et al. 1997). However, UV levels are
672 generally low below sea ice due to strong scattering in the snow package covering the
673 sea ice as well as in the ice itself, and UV-B levels are much lower than UV-A levels
674 (Perovich 1993). UV-B levels were not measured in the present study but can be
675 estimated based on a study of a comparable (~30 cm thick) sea ice Arctic sea ice (Winther
676 et al. 2004). That study showed that UV-B was about 100 times lower below the sea ice
677 compared to a measured UV-A of 3.7 W m^{-2}, which equals a maximum UV-B of 0.037 W
678 m^{-2} in the high light area. These are low levels and it is unlikely that UV-B was linked to
679 the observed changes in fatty acid composition. This is supported by a study where UV-
680 B reached about 1.0 W m^{-2} just below a water surface but with only limited effects on fatty
681 acid composition of the diatom *Thalassiosira antarctica* var. *borealis* in monoculture (Leu
682 et al. 2006). This diatom genus was also found below the ice in the present study but
683 could not be identified to species level. Indeed, the Leu et al. (2006) study identified PAR
684 as the main factor for observed changes in fatty acids compositions. This is in line with
685 our results, which showed that changes in relative compositions of PUFAs and MUFAs
686 were significantly higher in the 400% area. The maximum PAR levels in their experimental
687 aquarium reached about 300 µmol m^{-2} s^{-1} (Leu et al. 2006), and about two times higher
688 than the present study. It is ecologically significant that changes in fatty acid compositions
689 can be induced by even a small increase in under-ice PAR.

690

691

692 **4.5 The snow cover**

693 We show here the importance of a 5-10 cm thick snow cover and the various
694 photophysiological and photoprotective effects on the ice algae community at the bottom
695 of the ice if reduced or removed. Climate models predict increased precipitation in Arctic
696 regions, and thus higher snowfall (Bjorkman et al. 2015), whereas more recent models
697 predict that the increased precipitation will fall as rain (Peeters et al. 2019). However,
698 long-term (~50 years) actual measurements from the Arctic Ocean of snow depth have
699 shown a clear decrease in snow thickness, and especially in May (Warren et al. 1999).
700 Specific decreases in snow cover from 32.9 to 14.5 cm have been observed in the
701 Beaufort and Chukchi seas, and from 35.1 to 22.2 cm in the western Arctic (Webster et
702 al. 2014). The reduction was related to a later freeze up of the sea ice in autumn, and
703 thereby a reduced period for the snow to accumulate on the snow during the autumn
704 season with highest snowfall.

705

5. Conclusions

We emphasize here the importance of the snow cover as a regulator and moderator of surface irradiance available for ice algae and their photophysiology, biomass, pigment composition, and nutritional quality at the bottom of the sea ice in an Arctic ecosystem. Other studies have also identified the crucial role of the snow cover for various parameters, but this is the first time where all the above-mentioned parameters have been studied simultaneously. The response time (6 days) of the central photophysiological fluorescence yield parameter (Φ_{PSII_max}) was similar to the response time of the photoprotective parameters such as pigment composition and MAAs. Significant changes in fatty acid composition occurred at Day 12. The significant decreases in both photophysiological and photoprotective parameters were proportional to the increase in irradiance. After fourteen days of experiment, the ice algae were still able to down-regulate their photosynthetic machinery with increased irradiance, but ice algae exposed to higher (200% and 400%) irradiance showed clear signs of chronic photoinhibition.

Acknowledgements. Financial support is acknowledged to KH, LCLH, and BKS from the Danish Council for Independent Research (Project DFF –1323-00335: Sea ice ecosystems: Ecological effects of a thinning snow cover), Carlsberg Foundation Project CF14–0888 and the Brdr. Hartmann Foundation. Thanks to Rikka Møller at Kangerlussuaq International Science Support (KISS) for logistical assistance and support.

728

729 LITERATURE CITED

730

731 Arendt KE, Jonasdottir SH, Hansen PJ, Gartner S (2005) Effects of dietary fatty acids on
732 the reproductive success of the calanoid copepod Temora longicornis. Mar Biol 146: 513-
733 530

734

735 Arrigo KR, Dijken G, Pabi S (2008) Impact of a shrinking Arctic ice cover on marine
736 primary production. Geophys Res Let 35: L19603

737

738 Assmy P, Fernández-Méndez M, Duarte P, Meyer A, Randelhoff A, Mundy CJ, Olsen
739 LM, Kauko HM, Bailey A, Chierici M, Cohen L, Doulgeris AP, Ehn JK, Fransson A,
740 Gerland S, Hop H, Hudsonm SR, Hughes N, Itkin P, Johnsen GM, King JA, Koch BP,
741 Koening Z, Kwasniewski S, Laney SR, Nicolaus M, Pavlov AK, Polashenski CM, Provost
742 C, Rösel A, Sandbu M, Spreen G, Smedsrud LH, Sundfjord A, TaskjelleT, Tatarek A,
743 Wiktor J, Wagner PM (2017) Leads in Arctic pack ice enable early phytoplankton blooms
744 below snow-covered sea ice. Sci Rep 7, Article number: 40850

745

746 Ayoub LM, Hallock P, Coble PG, Bell SS (2012) MAA-like absorbing substances in Florida
747 Keys phytoplankton vary with distance from shore and CDOM: Implications for coral reefs.
748 J Exp Mar Biol Ecol 420-421: 91-98

749

750

751 Bjorkman AD, Elmendorf SC, Beamish AL, Vellend M, Henry GHR (2015). Contrasting
752 effects of warming and increased snowfall on Arctic tundra plant phenology over the past
753 two decades. Glob Chan Biol 21:4651-4661

754

755 Budge SM, Wooller MJ, Springer AM, Iverson SJ, McRoy CP, Divoky GJ (2008) Tracing
756 carbon flow in an arctic marine food web using fatty acid-stable isotope analysis.
757 Oecologia 157: 117-129

758

759 Campbell K, Mundy CJ, Barner DG, Gosselin M (2014) Characterizing the sea ice algae
760 chlorophyll a-snow depth relationship over Arctic spring melt using transmitted irradiance.
761 J Mar Sys 147: 76-84

762

763 Carreto JI, Carignan MO (2011) Mycosporine-like amino acids: Relevant secondary
764 metabolites. Chem Ecol Asp 9: 387-446

765

766 Cleveland JS, Weidemann AD (1993) Quantifying absorption by aquatic particles: A
767 multiple scattering correction for glass-fiber filters. Limnol Oceanogr 38(6): 1321-1327

Doreen K, Schaafsma FL, Graeve M, Lebreton B, Lange BA, David C, Vortkamp M, Flores H (2017) Strong linkage of polar cod (Boreogadus saida) to sea ice algae-produced carbon: Evidence from stomach content, fatty acid and stable isotope analyses. Prog Oceano152: 62-74

Elliott A, Mundy CJ, Gosselin M, Poulin M, Campbell K, Wang F (2015) Spring production of mycosporine-like amino acids and other UV-absorbing compounds in sea ice-associated algae communities in the Canadian Arctic. Mar Ecol Prog Ser 541: 91-104

Ficek D, Dera J, Wozniak B (2013) UV absorption reveals mycosporine-like amino acids (MAAs) in Tatra mountain lake phytoplankton. Oceanologia 55: 599-609

Fernández-Méndez M, Katlein C, Rabe B, Nicolaus M, Peeken I, Bakker K, Flores H, Boetius A (2015) Photosynthetic production in the central Arctic Ocean during the record sea ice minimum 2012. Biogeosci 12: 3525-3549

Galindo V, Gosselin M, Lavaud J, Mundy CJ, Else B, Ehn J, Babin M, Rysgaard S (2017) Pigment compistion and photoprotection of Arctic sea ice algae during spring. Mar Ecol Prog Ser 585:49-69

Garrison DL, Buck KR (1986) Organism losses during ice melting: A serious bias in sea ice community studies. Pol Biol 6: 237-239

Gosselin M, Levasseur M, Wheeler PA, Horner, RA, Booth BC (1997) New measurements of phytoplankton and ice algal production in the Arctic Ocean. Deep Sea Res II 44:1623-1644

Grasshoff K, Ehrhardt M, Kremling K (1983) Methods of seawater analysis. Second Editon. Weinheim/Deerfield Beach, Florida, Verlag Chemie, 419 pp

Grossi SMG, Kottmeier ST, Moe RL, Taylor GT, Sullivan CW (1987) Sea ice microbial communities. VI. Growth and primary production in bottom ice under graded snow cover. Mar Ecol Prog Ser 35: 153-164

Ha SY, Joo HM, Kang SH, Ahn IY, Shin KH (2014) Effect of ultraviolet irradiation on the production and composition of fatty acids in plankton in a sub-Antarctic environment. J Oceanography 70: 1-10

Hancke K, Lund-Hansen LC, Lamare ML, Pedersen SH, King MD, Andersen P, Sorrell BK (2018) Extreme low light requirement for algae growth underneath sea ice: A case study from station Nord, NE Greenland. J Geophys Res123: 985-1000

Haro S, Bohorquez J, Lara M, Garcia-Robledo E, Gonzalez CJ, Crespo JM, Papaspyrou S, Corzo A (2019) Diel patterns of microphytobenthic primary production in intertidal sediments: the role of photoperiod on the vertical migration circadian rhythm. Sci Rep 9, Article number: 13376

Hasholt B, Mikkelsen AB, Nielsen MH, Larsen MAD (2012) Observations of runoff and sediment and dissolved loads from the Greenland ice sheet at Kangerlussuaq, West Greenland, 2007 to 2010. Z f Geomorph 57: 1-25

Hawes I, Lund-Hansen LC, Sorrell BK, Nielsen MH, Borzák R, Buss I (2012) Photobiology of sea ice algae during initial spring growth in Kangerlussuaq, West Greenland: insights from imaging variable chlorophyll fluorescence of ice cores. Photosynth Res 112: 103-115

Helbling EW, Chalker BE, Dunlap WC, Holm-Hansen O, Villafane VE (1996) Photoacclimation of antarctic marine diatoms to solar ultraviolet radiation. J Exp Mar Biol Ecol 204: 85-101

Hessen DO, De Lange HJ, Donk EV (1997) UV-induced changes in phytoplankton cells and its effects on grazers. Freshw Biol 38: 513-524

Horner R (2018) Sea Ice Biota. Baco Raton, CRC Press, 223 pp

Hou Y, Liang W, Zhang L, Cheng S, He F, Wu Z (2011) Freshwater algae chemotaxonomy by high-performance liquid chromatographic (HPLC) analysis. Front Environ Sci Engin China 5(1): 84-91

Juhl AR, Krembs C (2010) Effects of snow removal and algal photoacclimation on growth and export of ice algae. Pol Biol 33: 1057-1065

Karentz D, McEuen FS, Land MC, Dunlap WC (1991) Survey of mycosporine-like amino acid compounds in Antarctic marine organisms: potential protection from ultraviolet exposure. Mar Biol 108: 157-166

Kauko HM, Olsen LM, Duarte P, Peeken I, Granskog MA, Johnsen G, Fernández-Méndez M, Pavlov AK, Mundy CJ and Assmy P (2018) Algal colonization of young Arctic sea ice in Spring. Front. Mar Sci 5:199

Laurion I, Blouin F, Roy S (2003) The quantitative filter technique for measuring phytoplankton absorption: Interference by MAAs in the UV waveband. Limnol Oceanogr: Methods 1: 1-9

852 Lavaud J, Goss R (2014) The peculiar features of Non-photochemical fluorescence
853 quenching in diatoms and brown algae. In: Non-photochemical quenching and energy
854 dissipation in plants, algae and cyanobacteria. (Demming-Adams B, Garab G, Govindjee
855 eds.). Advances in photosynthesis and respiration, Springer, Berlin, 643 pp
856
857 Leu E, Wangberg SÅ, Wulff A, Falk-Petersen S, Ørbæk JB, Hessen DO (2006) Effects of
858 changes in ambient PAR and UV radiation on the nutritional quality of an Arctic diatom
859 (*Thalassiosira antarctica* var. *borealis*). J Exp Mar Biol Ecol337: 65-81
860
861 Leu E, Wiktor J, Søreide JE, Berge J, Falk-Petersen S (2010) Increased irradiance
862 reduces food quality of sea ice algae. Mar Ecol Prog Ser 411: 49-60
863
864 Leu E, Mundy CJ, Assmy P, Campbell K, Gabrielsen TM, Gosselin M, Juul-Pedersen T,
865 Gradinger R (2015) Arctic spring awakening – Steering principles behind the phenology
866 of vernal ice algal blooms. Prog Oceano 139: 151-170
867
868 Lund-Hansen LC, Andersen TJ, Nielsen MH, Pejrup M (2010) Suspended matter, Chl-a,
869 CDOM, grain sizes, and optical properties in the Arctic fjord-type estuary, Kangerlussuaq,
870 West Greenland during Summer. Est and Coast 33: 1442-1451
871
872 Lund-Hansen LC, Hawes I, Sorrell BK, Nielsen MH (2014) Removal of snow cover inhibits
873 spring growth of Arctic ice algae through physiological and behavioral effects. Pol Biol 37:
874 471-481
875
876 Lund-Hansen LC, Hawes I, Nielsen MH, Sorrell BK (2016) Is colonization of sea ice by
877 diatoms facilitated by increased surface roughness in growing ice crystals? Pol Biol 40:
878 593-602
879
880 Lund-Hansen LC, Hawes I, Nielsen MH, Dahllof I, Sorrell BK (2018) Summer meltwater
881 and spring sea ice primary production, light climate and nutrients in an Arctic estuary,
882 Kangerlussuaq, West Greenland, Arctic, Antarc and Alp Res 50: 1, S100025
883
884 Lund-Hansen LC, Juul T, Eskildsen TD, Hawes I, Sorrell BK, Melvad C, Hancke K (2018a)
885 A low-cost remotely operated vehicle (ROV) with an optical positioning system for under-
886 ice measurements and sampling. Cold Reg Sci Tech 151: 148-155
887
888 Lund-Hansen LC, Bendtsen J, Stratmann T, Tonboe R, Olsen SM, Markager S, Sorrell
889 BK (2020) Will low primary production rates in the Amundsen Basin (Arctic Ocean) reamin
890 low in a future ice-free setting, and what governs this production? J Mar Sys (in print)
891
892 Mikkelsen DM, Rysgaard S, Glud RN (2008) Microalgal composition and primary
893 production in Arctic sea ice: a seasonal study from Kobbefjord (Kangerluarsunnguaq),
894 West Greenland. Mar Ecol Prog Ser 368: 65-74

Mitchell BG, Kahru M, Wieland J, Stramska M (2002) Determination of spectral absorption coefficients of particles, dissolved material and phytoplankton for discrete water samples – Chapter 15. In: Mueller, J.L., Fargion, G.S. (Eds.). Ocean Optics Protocols for Satellite Ocean Color Sensor Validation, Revision 3, Vol 2.

Mock T, Gradinger R (1999) Determination of Arctic algal production with a new in situ incubation technique. Mar Ecol Prog Ser 177: 15-26

Mundy CJ, Barber DG, Michel C (2005) Variability of snow and ice thermal, physical and optical properties pertinent to sea ice algae biomass during spring. J Mar Sys 58: 107-120

Mundy CJ, Ehn JK, Barber DG, Michel C (2007) Influence of snow cover and algae on the spectral dependence of transmitted irradiance through Arctic landfast first-year sea ice. J Geophys Res 112: C03007

Mundy CJ, Gosselin M, Ehn JK, Belzile CM, Poulin M, Alou E, Roy S, Hop H, Lessard S, Papakyriakou TN, Barber DG, Stewart J (2011) Characteristics of two distinct high-light acclimated algal communities during advanced stages of sea ice melt. Pol Biol 34: 1869-1886

Mundy CJ, Gosselin M, Gratton Y, Brown K, Galindo V, Campbell K, Levasseur M, Barber D, Papakyriakou T, Belanger S (2014) Role of environmental factors on phytoplankton bloom initiation under landfast sea ice in Resolute Passage, Canada. Mar Ecol Prog Ser 497: 39-49

Nicolaus M, Katlein C, Maslanik J, Hendricks S (2012) Changes in Arctic sea ice result in increasing light transmittance. Geophys Res Let 39, Issue 24

Nielsen MH, Erbs-Hansen DR, Knudsen KL (2010) Water masses in Kangerlussuaq, a large fjord in West Greenland: the processes of formation and the associated foraminiferal fauna. Pol Res 29: 159-175

Nymark M, Valle KC, Brembu T, Hancke K, Winge P (2009) An Integrated Analysis of Molecular Acclimation to High Light in the Marine Diatom Phaeodactylum tricornutum. Plos One 4(11): e7743

Pabi S, Dijken GL, Arrigo KR (2008) Primary production in the Arctic Ocean 1998-2006. J Geophys Res 113, C08005

Peeters B, Pedersen ÅØ, Loe LG, Isaksen K, Veiberg V, Stien A, Kohler J, Gallet J-C, Aanes R, Hansen BB (2019) Spatiotemporal patterns of rain-on-snow and basal ice high

Arctic Svalbard: detection of a climate-cryosphere regime shift. Environ Ress Lett 14:915002

Perovich D (1993) A theoretical model of ultraviolet light transmission through Antarctic sea ice. J Geophys Res 98: 22579-22587

Perovich DK (2017) Sea ice and sunlight, 110-137. In: Sea Ice (ed. Thomas, D.N.), 3rd edition. Wiley Blackwell, UK, 652 pp

Petrou K, Doblin MA, Ralph PJ (2011) Heterogeneity in the photoprotective capacity of three Antarctic diatoms during short-term changes in salinity and temperature. Mar Biol 158: 1029-1041

Piiparinen J, Enberg S, Rintala JM, Sommaruga R, Majaneva M, Autio R, Vahatalo AV (2015) The contribution of mycosporine-like amino acids, chromophoric dissolved organic matter and particles to the UV protection of sea-ice organisms in the Baltic Sea. Photochem Photobiol Sci 14:1025-1034

Platt T, Gallegos C L, Harrison W G (1980) Photoinhibition of photosynthesis in natural assemblages of marine phytoplankton. J M Res 38: 687-701

Ralph PJ, Gademann R (2005) Rapid light curves: A powerful tool to assess photosynthetic activity. Aquat Bot 82: 222-237

Reuss N, Poulsen LK (2002) Evaluation of fatty acids as biomarkers for a natural plankton community. A field study of a spring bloom and a post-bloom period off West Greenland. Mar Biol141: 423-434

Riegger L, Robinson D (1997) Photoinduction of UV-absorbing compounds in Antarctic diatoms and Phaeocystis antarctica. Mar Ecol Prog Ser 160: 13-25

Rintala JM, Piiparinen J, Blomster J, Majaneva M, Muller S, Uusikivi J, Autio R (2014) Fast direct melting of brackish sea-ice samples results in biologically more accurate results than slow buffered melting. Polar Biol 37: 1811-1822

Rysgaard S, Kühl M, Glud RN, Hansen JW (2001) Biomass, production and horizontal patchiness of sea ice algae in a high-Arctic fjord (Young Sound, NE Greenland). Mar Ecol Prog Ser 223: 15-26

Sargent JR, Bell MV, Bell JG, Henderson RJ, Tocher DR, (1995) Evolution and roles of (n-3) polyunsaturated fatty acids in marine organisms. In: Phospholipids: Charaterization, Metabolism and Novel Biological Applications. Am Oil Chem Soc Press. Champaign, Illinois, USA, 248-259 pp

Schreiber U, Schliwa U, Bilger W (1986) Continuous recording of photochemical and nonphotochemical chlorophyll fluorescence quenching with a new type of modulation fluorometer. Photosynth Res 10: 51–62

Schreiber U (2004) Pulse-Amplitude-Modulation (PAM) fluorometry and saturation pulse method: an overview. In: Papageorgiou GC, Godvindjee (eds.) Chlorophyll a fluorescence: a signature of photosynthesis. Kluwer Academic Publishers, Dordrecht, The Netherlands, 279–319 pp

Shick JM, Dunlap WC (2002) Mycosporine-Like aminoacids and related gadusols: Biosynthesis, accumulation, and UV-protective functions in aquatic organisms. An Rev Physio 64:223-262

Sinha RP, Singh SP, Hader DP (2007) Database on mycosporines and mycosporine-like amino acids (MAAs) in fungi, cyanobacteria, macroalgae, phytoplankton and animals. J Photochem Photobiol B: Biology 89: 29-35

Thompson PA, Guo M, Harrison PJ, Whyte JNC (1992) Effects of variation in temperature. II. On the fatty acid composition of eight species of marine phytoplankton. J Phycol 28: 488-497

Utermöhl H (1958) Zur Vervollkommung der quantitativen Phyto-plankton Methodik. Mitt Der Int Verein für Limno 9: 1-39

Vosjan JH, Dohler G, Nieuwland G (1990) Effect of UV-B irradiance on the ATP content microorganisms of the Weddell sea (Antarctica). Netherlands J Sea Res 25: 391-393

Wang KS, Chai T (1994) Reduction in omega-3 fatty acids by UV,B irradiation in microalgae. J Appl Phycol 6: 415-421

Warren SG, Rigor IG, Untersteiner N, Radionov VF, Bryazgin NN, Aleksandrov YI, Colony R (1999) Snow depth on Arctic sea ice. J Climate 12: 1814-1829

Webster MA, Rigor IG, Ngheim SV, Kurtz NT, Farrell SL, Perovich DK, Sturm M, (2014) Interdecadal changes in snow depth on Arctic sea ice. J Geophys Res Oceans 119:5395-5406

Winther JG, Edvardsen K, Gerland S, Hamre B, (2004) Surface reflectance of sea ice and under-ice irradiance in Kongsfjord, Svalbard. Pol Res 23:115-118

1022 Table 1. Two-way ANOVA analysis of chl *a*, variable chlorophyll fluorescence, and
1023 MUFA:PUFA ratio data from algae in the lower 3 cm of sea ice cores, with treatment as
1024 a fixed factor and time as a random factor. Significant differences ($P < 0.05$) shown in
1025 **bold**.

Source	d.f.	MS	*F*	*P*
Chl *a*				
Treatment	2	0.0275	9.92	**0.0009**
Treatment ×	10		3.58	**0.0005**
Date		0.0014		
Treatment	2	0.195	77.10	**< 0.0001**
Treatment ×	10		11.77	**< 0.0001**
Date		0.0029		
A				
Treatment	2	0.0013	5.00	**0.0134**
Treatment ×	8		3.25	**0.0089**
Date		0.0008		
E_k				
Treatment	2	1866.35	3.22	0.0541
Treatment ×	8		1.75	0.1267
Date		1016.30		
$rETR_{max}$				
Treatment	2	19.38	4.73	**0.0164**
Treatment ×	8		1.14	0.3683
Date		4.66		
PUFA:MUFA ratio				
Treatment	2	0.0989	9.75	**0.0038**
Treatment ×	10		1.41	0.2256
Date		0.1566		
Diel Φ_{PSII} variation				
Treatment	2	0.1995	321.92	**< 0.0001**
Treatment ×	14		2.35	**0.0158**
Time		0.0015		

1026

1027

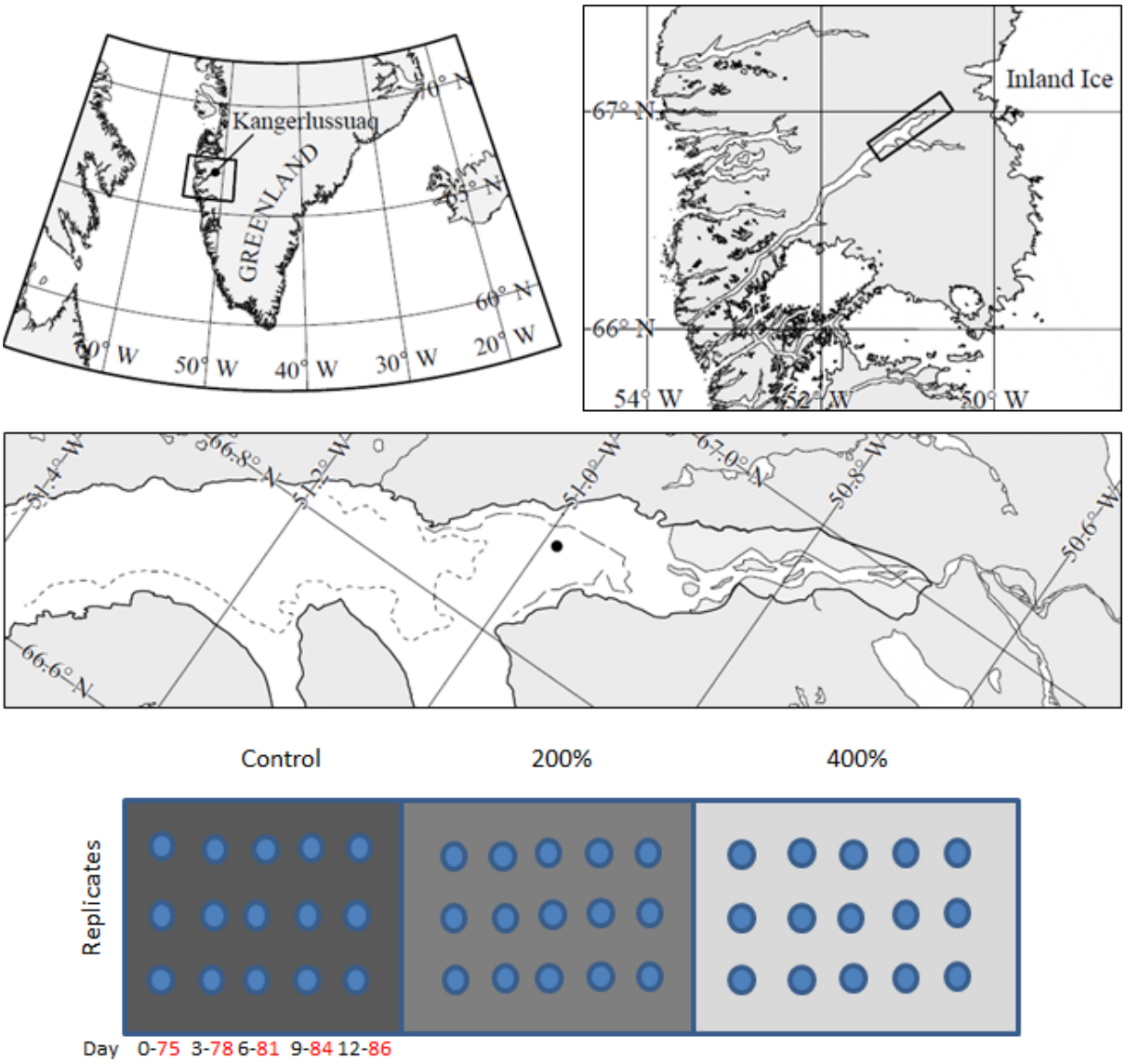

Fig. 1. Area of study and sampling design for sea ice coring at Kangerlussuaq Fjord, Greenland. Sampling was laid out as a runway along a southwest to northeast runway with three discrete experimental areas differing in light transmission and under-ice irradiance. Treatments: (i) a control low light area with undisturbed snow cover; (ii) an area with 200% (doubled) irradiance (all snow removed, ice covered with a 50% transmission shade cloth); and (iii) an area with 400% irradiance (all snow removed). The 200% and 400% irradiance areas were re-cleared daily of any snowdrift throughout the experiment. Three replicate cores were collected from each area over a 12-day period at intervals as shown schematically with Julian Days in red.

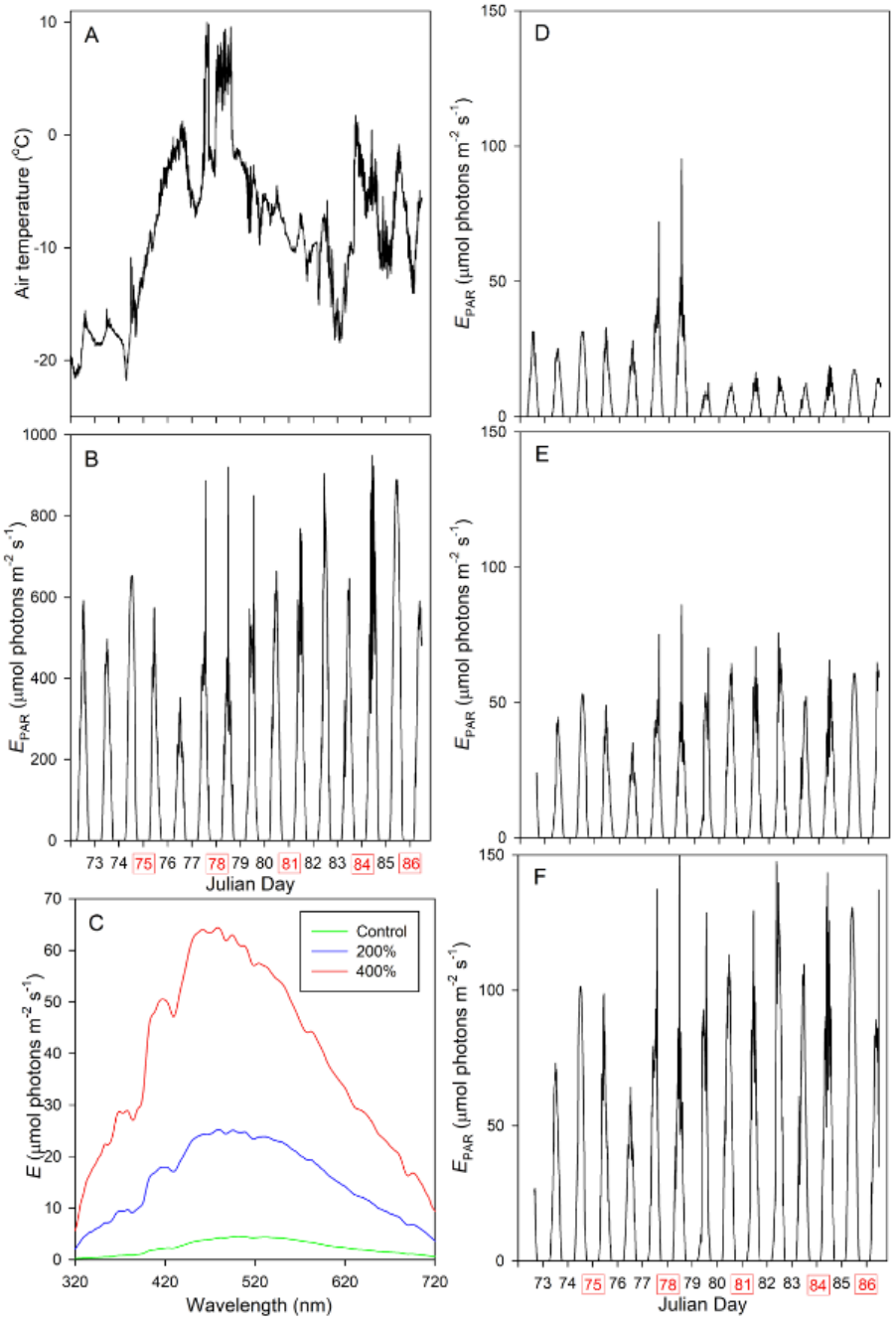

Fig. 2. Records of physical data describing temperature and light conditions at the sampling area on Kangerlussuaq Fjord during the experiment. (A) Air temperature. (B) Downwelling irradiance. (C) Comparison of spectral distribution of irradiance between the three experimental areas, *viz:* control (undisturbed snow), 200% irradiance (shade cloth), and 400% irradiance (snow cleared) treatments. The under-ice PAR logged *in situ* for the three experimental areas is shown for the (D) control, (E) 200%, and (F) 400% treatments. Sampling days (3, 6, 9, 12, 14) shown in red text.

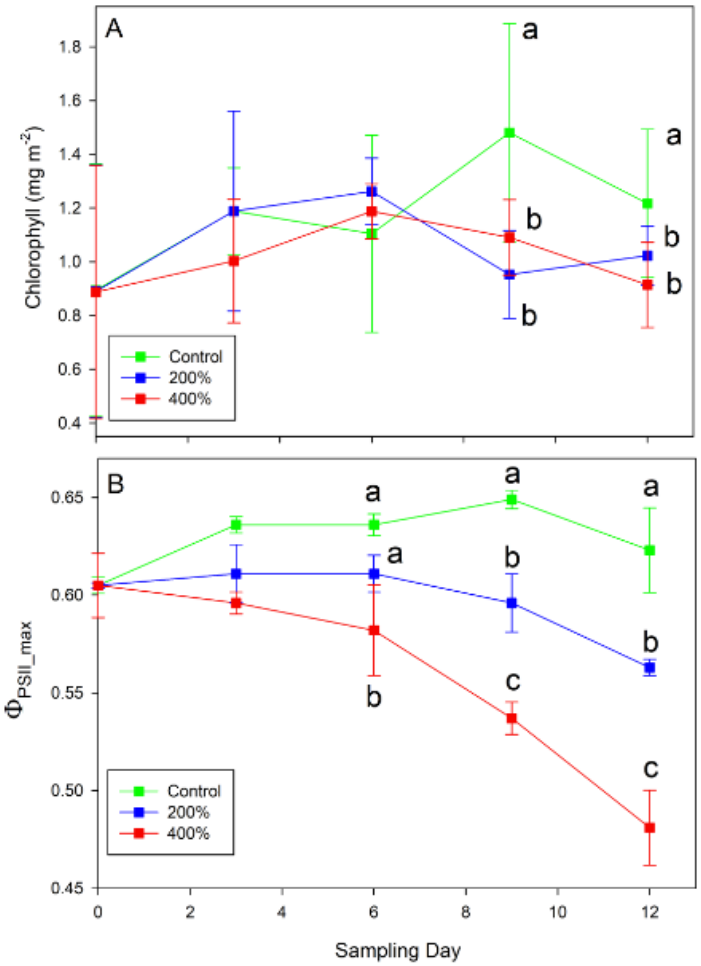

Fig. 3. Time series of differences between the three treatments (control, 200% and 400% irradiance) in development of (A) chl-*a* on underside of sea-ice; and (B) Phyto-PAM estimation of ice algal maximum dark-adapted fluorescence yield (Φ_{PSII_max}) during the experiment. Mean values in (A) and (B) (n=3) ± 1SD; treatments sharing letters are not significantly different (Tukey's *post hoc* honestly significantly difference tests, $P < 0.05$).

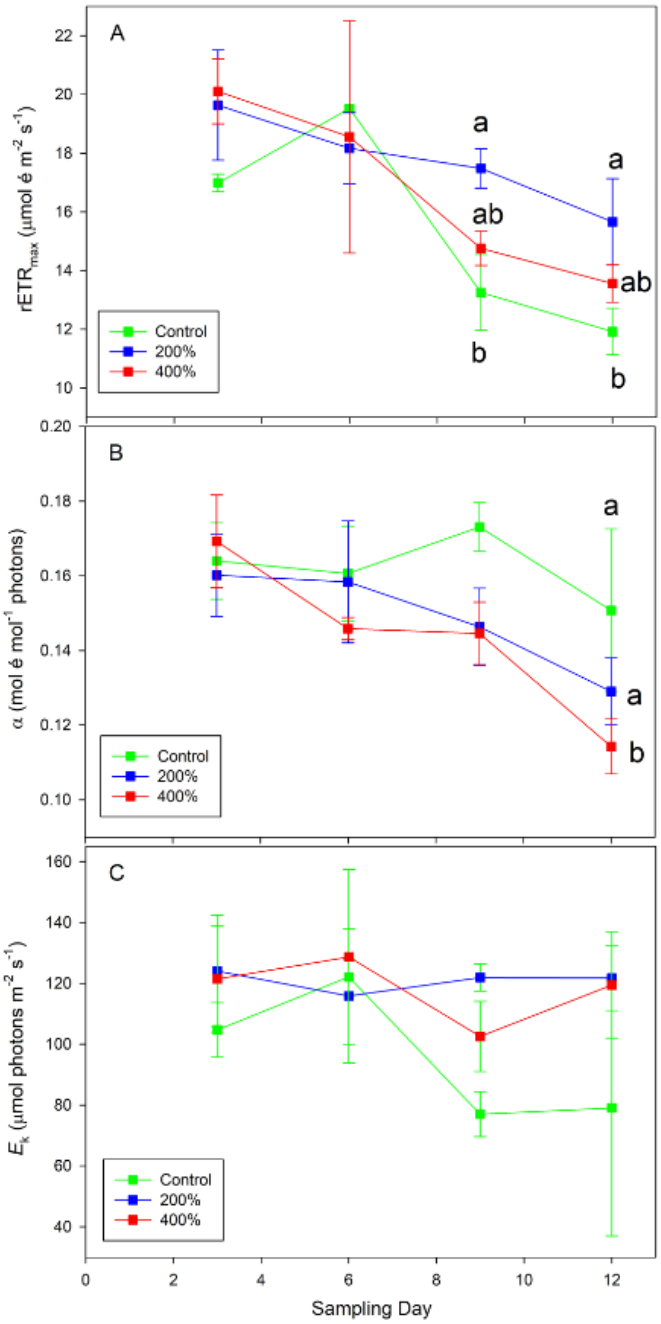

Fig. 4. Time series of differences between the three treatments (control, +200% and +400% irradiance) in development of light acclimation parameters from Phyto-PAM rapid light curves; (A) the light-saturated relative electron transport rate ($rETR_{max}$ ($rETR = \Phi_{PSII} \times E_{PAR}$), (B) the initial slope α, and (C) the onset of light saturation E_k. Mean values (n=3) ± 1SD. Treatments sharing letters are not significantly different (Tukey's *post hoc* honestly significantly difference tests, $P < 0.05$).

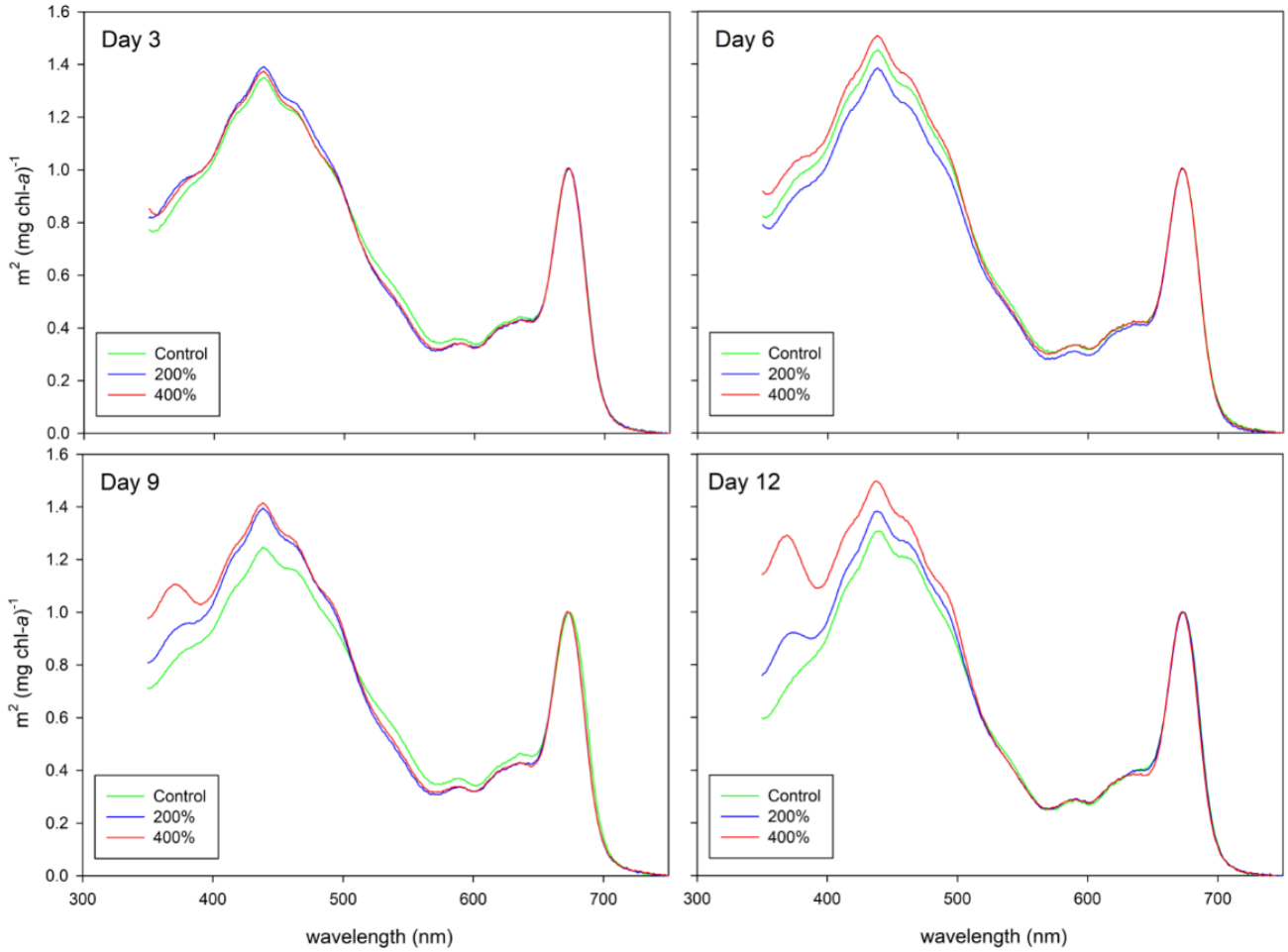

Fig. 5. Differences in chl-*a* specific absorption spectra of sea ice algae between the three treatments (control, 200% and 400% irradiance) on four sampling days during the experiment. Note similarity of spectra early in the experiment (Day 3) and progressive development of an additional absorption peak between 350 and 400 nm and at the blue-absorption peak on Days 9 and 12.

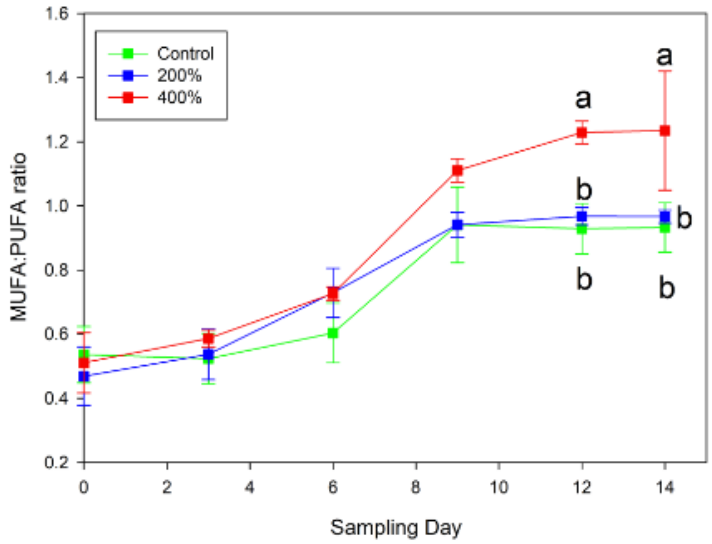

Fig. 6. Time series of differences between the three treatments (control, 200% and 400% irradiance) in development of the ratio of mono- to poly-unsaturated fatty acids in sea ice algal biomass. Mean values (*n*=3) ± 1SD; treatments sharing letters are not significantly different (Tukey's *post hoc* honestly significantly difference tests, $P < 0.05$).

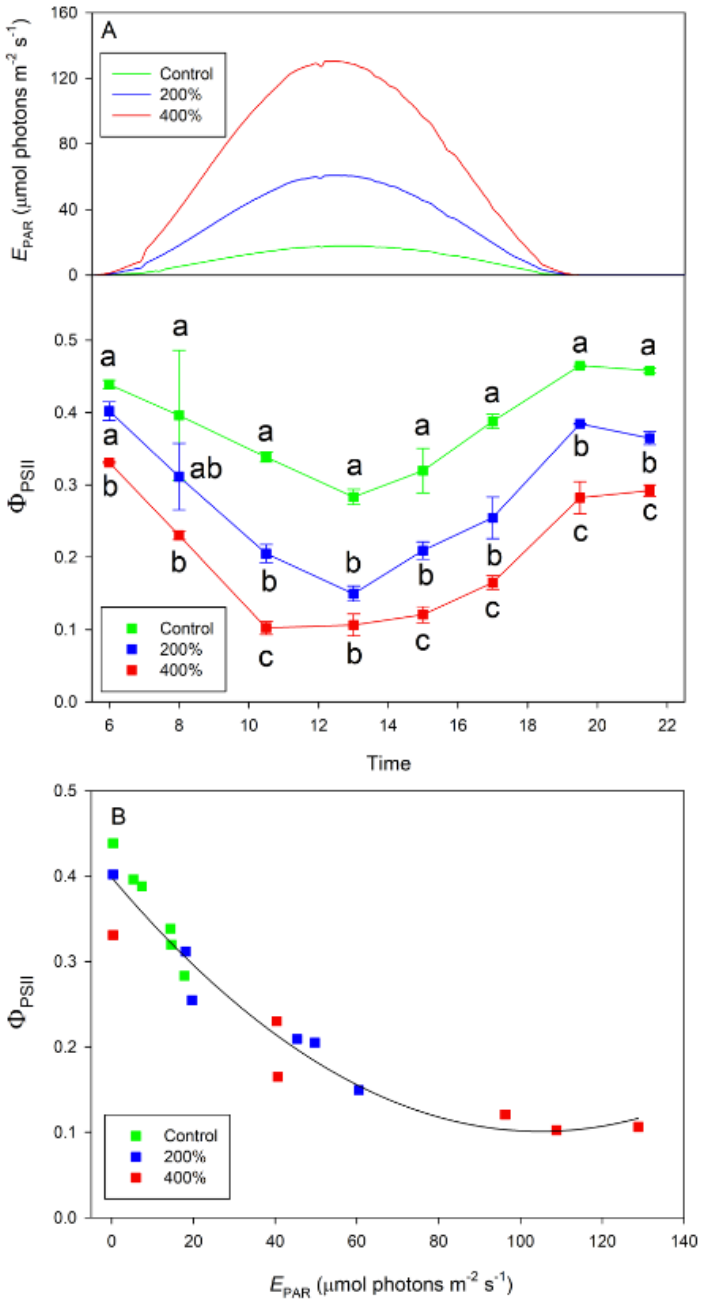

Fig. 7. (A) Comparison of differences between the three treatments (control, 200% and 400% irradiance) in diel cycles of the photosynthetic efficiency Φ_{PSII}, as measured directly *in situ* from immediately collected ice cores in the field using fluorescence imaging on Day 14 of the experiment. Mean values (n=3) ± 1SD, with under-ice PAR for Day 14 shown in upper panel. Treatments sharing letters are not significantly different (Tukey's post hoc honestly significantly difference tests, $P < 0.05$). (B) Data from (A) plotted as a function of under-ice irradiance as recorded by *in situ* light loggers at the time of sample collection showing exponential decrease of Φ_{PSII} with irradiance.